Journal of Neuroscience Methods 330 (2020) 108505

Contents lists available at ScienceDirect

Journal of Neuroscience Methods

journal homepage: www.elsevier.com/locate/jneumeth

# Localization of movable electrodes in a multi-electrode microdrive in nonhuman primates

Elsie Premereur[a,*,1], Thomas Decramer[a,b,1], Walter Coudyzer[c], Tom Theys[b], Peter Janssen[a]

[a] Laboratory for neuro- and psychophysiology and the Leuven Brain Institute, KU Leuven, Herestraat 49, 3000 Leuven, Belgium
[b] Laboratory for experimental neurosurgery and neuroanatomy and the Leuven Brain Institute, KU Leuven, Herestraat 49, 3000 Leuven, Belgium
[c] Department of Radiology, University Hospitals Leuven, Herestraat 49, 3000 Leuven, Belgium

ARTICLE INFO

*Keywords:*
Multi-electrode microdrive
Large-scale recording systems
Electrode localization
Computed tomography
Nonhuman primate

ABSTRACT

*Background:* Recently, large-scale semi-chronic recording systems have been developed, unique in their capability to record simultaneously from multiple individually moveable electrodes. As these recording systems can cover a large area, knowledge of the exact location of each individual electrode is crucial. Currently, the only method of keeping track of electrode depth and thus location is through detailed notebook keeping on neural activity.

*New Method:* We have improved the electrode localization by combining pre- and postoperative anatomical magnetic resonance imaging (MRI) scans with high resolution computed tomography (CT) scans throughout the experiment, and validated our method by comparing the resulting location estimates with traditional notebook-keeping. Finally, the actual location of a selection of electrodes was marked at the end of the experiment by creating small metallic depositions using electrical stimulation, and thereby made visible on MRI.

*Results:* Combining CT scans with a high resolution, artefact reducing sequence during the experiment with a preoperative MRI scan provides crucial information about the exact electrode location of multielectrode arrays with individually moveable electrodes.

*Comparison with Existing Methods:* The information obtained from the hybrid CT-MR image and the notes on spiking activity showed a similar pattern, with the clear advantage of the visualization of the exact position of the electrodes using our method.

*Conclusions:* The described technique allows for a precise anatomical identification of the recorded brain areas and thus to draw strong conclusions about the role of each targeted cortical area in the behavior under study.

## 1. Introduction

A widely used technique to measure neural activity in awake, behaving monkeys is to implant a recording chamber over a craniotomy and to lower an electrode into the brain on a daily basis (e.g.Premereur et al., 2011; Theys et al., 2012; Romero et al., 2014; Caprara et al., 2018). Although this method has proven highly successful and has also been used to compare the neuronal properties of multiple cortical areas (Snyder et al., 1997; Lawrence and Snyder, 2006; Verhoef et al., 2011; Theys et al., 2013), a crucial disadvantage is that it does not allow simultaneous recordings in multiple cortical areas. Multi-electrode recording systems allow to measure neural activity from several cortical and even subcortical areas simultaneously. Unfortunately, many of the currently available multi-electrode recording arrays are small, with short electrodes that can often not be moved. Recently, large-scale semi-chronic recording systems have been developed (Gray et al., 2007; Dotson et al., 2015, 2017), unique in their capability to record simultaneously from multiple individually moveable electrodes. As these recording systems can cover a large area, knowledge of the exact location of each individual electrode is crucial. However, keeping track of the electrode depth, together with detailed notes about transitions between background activity (gray matter) and silence (white matter and sulci) is currently the only way to estimate the location of the electrode tip. We have improved the electrode localization by combining computed tomography (CT) scans throughout the experiment with pre- and postoperative anatomical MRI scans, and validated our method by comparing the resulting location estimates with traditional notebook-keeping.

* Corresponding author at: Laboratory for neuro- and psychophysiology, KU Leuven, ON2, Herestraat 49, 3000 Leuven, Belgium.
*E-mail addresses:* elsie.premereur@kuleuven.be (E. Premereur), thomas.decramer@kuleuven.be (T. Decramer), walter.coudyzer@uzleuven.be (W. Coudyzer), tom.theys@kuleuven.be (T. Theys), peter.janssen@kuleuven.be (P. Janssen).
[1] Contributed equally to the manuscript.

https://doi.org/10.1016/j.jneumeth.2019.108505
Received 3 July 2019; Received in revised form 4 November 2019; Accepted 7 November 2019
Available online 08 November 2019

CT-MRI fusion is routinely performed in neurosurgery to localize intracranial electrodes (Darcey and Roberts, 2010) such as stereoelectroencephalography (sEEG) electrodes (Dykstra et al., 2012; Hinds et al., 2018), electrocorticography (ECoG) grids (Fujimoto et al., 2017) or deep brain stimulation (DBS) electrodes (Lee et al., 2010; Geevarghese et al., 2016; Engelhardt et al., 2018). In these patients electrode contacts of macroelectrodes, with a contact size and inter-contact spacing of several mm are localized, with different macro-electrodes inserted several centimeters apart. To date however, no study has combined high-resolution CT with MRI to localize individual electrodes in a multielectrode recording system with individually moveable electrodes, spaced only 1.5 mm apart.

In the current report we illustrate the localization of micro-electrodes with a thickness of 125 µm, 1.5 mm apart. To this aim, the CT sequence was optimized to reduce the artefact caused by the tungsten electrodes.

Finally, the actual location of a selection of electrodes was marked at the end of the experiment by creating small metallic depositions using electrical stimulation, and thereby made visible on MRI (Fung et al., 1998). Comparing the locations of the depositions with the estimations based on our CT/MRI technique validated our proposed method. Our results indicate that CT scanning using optimized scanning sequences provides important evidence about electrode location when using multielectrode recording systems with individually movable electrodes. The latter is crucial information when targeting different cortical areas, especially when separated by sulci.

## 2. Materials and methods

We implanted 3 monkeys with 4 semi-chronic 96 channel multi-electrode microdrives with glass-coated tungsten electrodes (Gray Matter research, Bozeman, United States; (Gray et al., 2007)); 2 in parietal and 2 in frontal cortex. All experimental procedures were performed in accordance with the National Institute of Health's Guide for the Care and Use of Laboratory Animals and EU Directive 2010/63/EU, and were approved by the Ethical Committee at KU Leuven. The animals in this study were pair or group-housed with cage enrichment (toys, foraging devices) at the primate facility of the KU Leuven Medical School. They were fed daily with standard primate chow supplemented with nuts, raisins, prunes and fresh fruits.

### 2.1. Preoperative MRI

Preoperative magnetic resonance imaging (MRI) was performed in a 3T scanner (Siemens Trio, Forchheim, Germany) while the animals were sedated with a mixture of ketamine (Nimatek, Eurovet; 12.5 mg/30 min) and medetomidine (Domitor, Orion; 0.25 mg/30 min).

The animals were positioned in a stereotactic frame (Kopf Model 1430 M, Tujunga, Canada) to allow precise calculation of the coordinates for the recording cylinders. To obtain high quality structural scans, three T1 MPRAGE volumes were collected and averaged (144 horizontal slices; 0.6 $mm^3$ isotropic voxels; TR: 2700 ms; TE: 3.8 ms; TI: 850 ms; flip angle: 90). MPRAGE images were collected with a receive-only custom-designed surface coil using the standard body transmitter (total scanning duration: 30 min). The preoperative scans were used to determine the exact location of the Gray microdrive (Fig. 1). A region of interest (ROI) was manually drawn on the resulting structural scan, allowing us to visualize which areas could be reached with the microdrive. Afterwards, the manufacturer built a 3D skull model, which allowed for a custom-made cylinder and microdrive, fitting perfectly on the skull.

### 2.2. Postoperative MRI

In a first surgical procedure, we implanted the cylinder (without microdrive or electrodes) using coordinates derived from the anatomical MRI and placement of the ROI (see 2.1). At our request, a plug was designed with four reference holes (Fig. 2A; anterior, lateral, medial and posterior). In monkey S holes were small and allowed for the insertion of 0.5 mm diameter glass tubes (FHC, Bowdoin, ME, USA) containing a 1% CuSO4 solution; in monkey A they were larger (1.5 mm) allowing to fill them with diluted gadolinium (5% solution of Dotarem 0.5 mmol/mL (Guerbet, Villepinte, France)). CuSO4 or gadolinium served as a contrast agent in a first postoperative MRI scan. This scan was used to estimate the area covered by the microdrive (monkey S over parietal cortex, monkey A over frontal cortex). After verification of the position of the cylinder, a craniotomy was performed which was closed with the plug, as per the manufacturer's guidelines. After recovery, the microdrive (with electrodes) was inserted in the cylinder, and electrodes were lowered through the dura to reach cortical areas (based on the presence of action potential activity).

### 2.3. Postoperative CT

After lowering part of the electrodes, we obtained computed tomography (CT) images of the brain using a high resolution CT scanner (Siemens Somatom Force, Forchheim, Germany; slice thickness 0.6 mm, increment 0.3 mm, kV 120, mAs 250, collimation: 64 × 0.6 mm helical CT, pitch: 0.85). The CT sequence was optimized to reduce metal artefacts caused by the electrodes and screws of the microdrive. This high-resolution CT visualizes individual electrodes and electrode tips (Fig. 3A). Importantly, the entire microdrive (electrodes, guiding tubes and the screws used to lower the electrodes) was visible on the CT volume, and allowed to follow and identify each individual electrode. Over the course of the experiment, the electrodes were lowered towards cortical areas of interest. On average, we recorded for 4 months in each animal while lowering electrodes, and every 4 weeks a new CT scan was performed to evaluate electrode depths.

The same stereotactic frame was used for both the CT and MRI imaging (Kopf Model 1430 M, David Kopf Instruments, Tujunga, Canada), allowing a perfect co-registration between both scans. After verification of the co-registration (using SPM12), a hybrid image was created using the imcalc tool in SPM12 (Fig. 3B). The latter image allows to visualize the individual electrodes from the CT scan on top of the T1 structural MRI. Hybrid images were created for all CT scans during the experiment (always using the same preoperative MR image), allowing us to keep track of the electrode depth (as measured on the CT scans) during the experiment together with meticulous notes of electrode depth expressed as the number of rotations of the screw driving the electrode down.

### 2.4. Notebook keeping

Throughout the experiment, detailed notes were kept on which electrodes were lowered; how much they were lowered; and the recorded activity (background activity, spikes, silence). Typically, half of the electrodes were lowered at the beginning of every recording session; the other half would be lowered during the next session, and so forth. Electrodes were lowered only 250 micron per session (after puncturing the dura). Note that, if necessary, electrodes were selected to be lowered more in the beginning of the experiment to allow simultaneous recordings of multiple cortical areas located at different distances from the dura. In an overview document, we indicated per recording session the actual depth of each electrode together with the kind of activity present.

### 2.5. Metallic depositions

To validate the accuracy of the MRI/CT hybrid images, we created small metallic depositions at the tip of a few selected (tungsten) electrodes by electrical stimulation. The depositions were visible on MRI scanning after removal of the microdrive, similar to depositions created

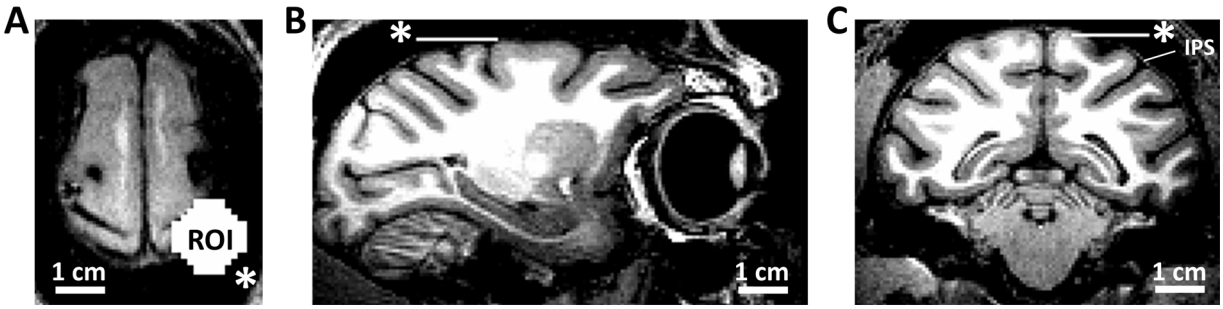


**Fig. 1.** Microdrive position is planned on an anatomical MRI (A: axial, B: sagittal, C: coronal) on which a region of interest (ROI) is drawn. The ROI (*) predicts the coverage of the multi-electrode system. The ROI and anatomical MRI are used to design a custom cylinder and microdrive. In this monkey we targeted areas around the intraparietal sulcus (IPS).

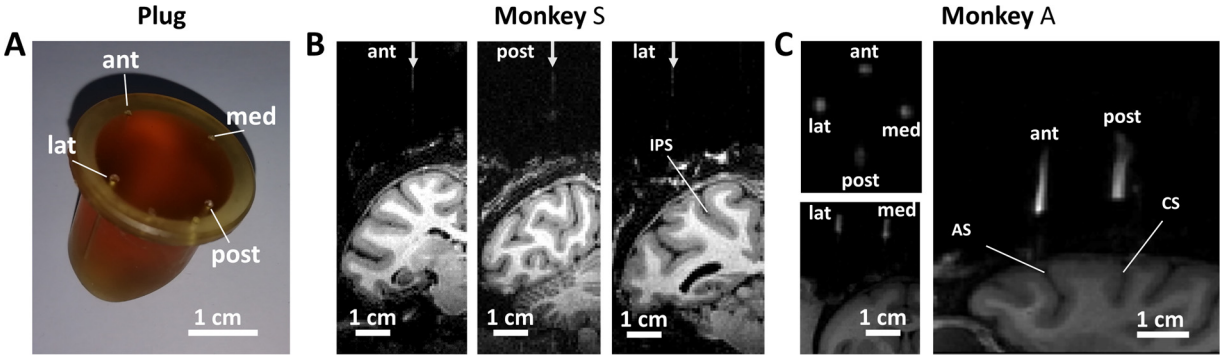


**Fig. 2.** Verification of cylinder position. (A) After the chamber is surgically implanted, a plug is inserted with holes in the anterior (ant), posterior (post), lateral (lat) and medial (med) positions. (B) Small holes (0.5 mm) allow to insert CuSO4-filled glass tubes, as in monkey S (parietal cortex). Figure demonstrates the tubes in respectively the anterior, posterior and lateral hole in the same cylinder. (C) Larger holes (1.5 mm) allow to fill the holes with gadolinium, as shown in monkey A (frontal cortex). Upper left: top view of the four holes. Lower left: coronal view showing lateral and medial holes. Right: sagittal view showing anterior and posterior holes. These images allow to estimate the area covered by the microdrive before making the craniotomy. IPS: intraparietal sulcus, AS: arcuate sulcus, CS: central sulcus.

after electrical stimulation of stainless steel electrodes (Fung et al., 1998). We injected current (40 µA 40 s; using a DS8000 stimulator in combination with current isolator DLS100, World Precision Instruments, Sarasota, USA) in 5 electrodes (monkey S) at the end of the experiment before retracting the electrodes and removing the microdrive. These five electrodes were selected based on their location in the microdrive as well as on functional findings during the experiment.

## 3. Theory

Understanding how several cortical (sub)areas respond during the same cognitive task at the same moment in time is one of the major challenges in neuroscience. Large-scale recordings allow to investigate in detail if different areas are involved in the same phases of a task and ultimately to obtain knowledge about how information travels through the brain (Umilta et al., 2007; Buschman and Miller, 2009). Furthermore, simultaneous recordings in multiple areas provides crucial information about the coherence between these cortical regions, which may indicate how these areas communicate, and about changes in coherence during different planning and execution phases of the task (Buschman and Miller, 2009; Verhoef et al., 2011).

The need to record simultaneously from a large number of neurons has led to several technological developments. Linear probes allow recordings from multiple contact points along their shaft and provide an excellent opportunity to record from several cortical layers simultaneously (Kaliukhovich and Vogels, 2012; Poort et al., 2016; Bastos et al., 2018; Takeda et al., 2018). Furthermore, arrays composed of multiple individual micro-wires (Fries et al., 1997; Roelfsema et al.,

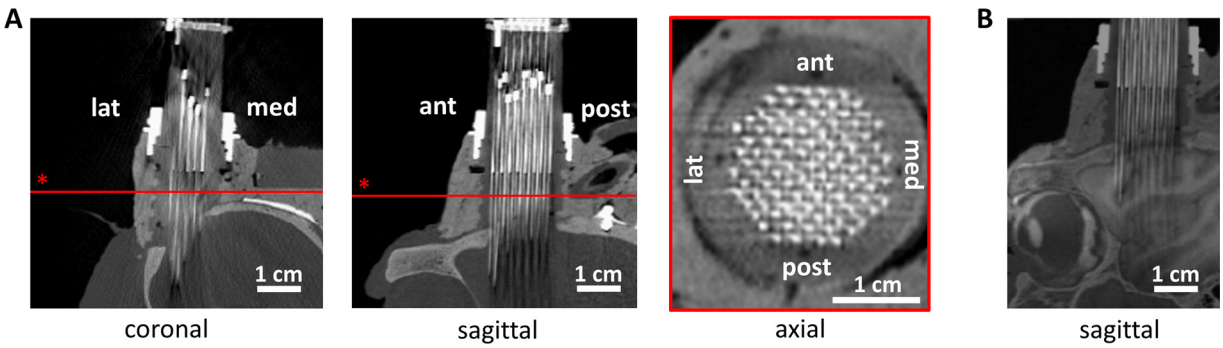


**Fig. 3.** Postoperative CT scans. (A) Native CT images allow tracking of individual electrodes due to artefact reduction. An axial slice (*, red line on coronal and sagittal CT image) through the microdrive illustrates all 96 electrodes, and each individual electrode can be identified and tracked further down until the electrode tip. (B) CT image overlay on preoperative anatomical MRI allowing both the individual electrodes and underlying brain structures to be visualized.

1997; Donoghue et al., 1998), arrays of rigidly linked micro-wires (Nicolelis et al., 1997, 2003; Musallam et al., 2007), or fabricated silicon electrode arrays (Nordhausen et al., 1996; Maynard et al., 1999; Rousche et al., 2001; Kipke et al., 2003; Kim et al., 2006; Dickey et al., 2009) have been developed. Although the latter methods have greatly improved our knowledge on cortical processing, they also suffer from specific limitations. Once these electrodes are in place, they can no longer be repositioned to isolate other individual neurons or to move into deeper structures. Thus, the experimenter can only access and thus study one set of neurons, and if neuronal activity on a particular electrode is not well isolated, or the signal is lost, that electrode can no longer yield useful data.

A second approach has utilized miniature microdrives that allow the implantation and positional control of large numbers of microelectrodes. Some methods enable position control for each individual probe (Wilson and McNaughton, 1993; de Charms et al., 1999; Erickson and Desimone, 1999; Venkatachalam et al., 1999; Swadlow et al., 2005; Eliades and Wang, 2008; Kloosterman et al., 2009; Nguyen et al., 2009), while others employ single or multiple devices to position arrays of electrodes together (Csicsvari et al., 2003; Krupa et al., 2004; Schwarz et al., 2014; Mendoza et al., 2016). Both approaches have been effective, but in general, most of the microdrives have been designed to manipulate a relatively small number of closely spaced probes, limiting the number of neurons and brain regions that can be simultaneously recorded from (see (Hoffman and McNaughton, 2002), (Feingold et al., 2012), and (Schwarz et al., 2014) for notable exceptions). To overcome the problems inherent to the approaches described above, large-scale recording devices with individually moveable electrodes have been developed (Gray et al., 2007; Dotson et al., 2015, 2017).

To target cortical areas of interest in macaque monkeys, the location of the craniotomy was originally calculated mainly based on stereotactic coordinates (Gross et al., 1972; Colby et al., 1996), more recently accompanied by MRI scanning for verification (Janssen et al., 1999; Scherberger et al., 2003). MRI scanning with an electrode targeted towards the 'neuronal hotspot' even allows the exact localization of neuronal responses (Tsao et al., 2006; Premereur et al., 2016; Caprara et al., 2018). A similar technique can be used for the implantation of multielectrode recording systems, in which the chamber positioning is often crucial to allow recordings from as many different cortical areas as required. The experimenter will localize the cortical regions of interest on an MRI scan and ascertain the stereotactic position of the chamber (Fig. 1). It is however impossible to localize individual electrodes of a chronically implanted microdrive system during the experiment using MRI due to the presence of metal in the microdrive, thus the actual precise location of the electrodes (mediolateral, anteroposterior and dorsoventral) cannot be verified. Information about electrode locations is crucial, as neuronal properties can change drastically and sometimes without any clear anatomical border. For example, when moving from the most anterior part of the lateral bank of the intraparietal sulcus to the more posterior part, neuronal response properties change from grasping related to eye movement related responses (Colby et al., 1996; Murata et al., 2000; Nelissen and Vanduffel, 2011; Premereur et al., 2012; Romero et al., 2014); while the medial bank of the intraparietal sulcus is implicated in reaching (Snyder et al., 1997).

It is especially challenging to keep track of the electrode depth throughout the experiment, when the electrodes are typically lowered on a daily basis, or in case the experimenters want to lower certain electrodes faster than others in order to record simultaneously from different areas. Knowing the exact electrode depth is crucial when the electrodes pass through several cortical areas, delineated by white matter or a sulcus. Typically, the electrode depth for multielectrode recording devices with individual moveable electrodes is measured relative to the dura, and the neural signal gives information about the tissue the electrode is currently recording from (spiking activity in gray matter, no activity in the white matter or the sulcus). Thus, in order to determine the exact electrode location one needs to know the depth at which the dura was punctured; the actual depth of each electrode; and the changes in neural signal indicating gray matter versus sulcus or white matter. Unfortunately, several factors can complicate the exact determination of the location of the electrode tip. The depth at which the electrode picks up neuronal activity for the first time is determined as the depth at which the dura is punctured. (Note that puncturing the dura is also accompanied by a change in impedance of the electrode leading to a signal change: the signal amplitude will typically decrease when the electrode hits the dura and increase again after the dura has been punctured). It is however not always possible to determine the exact moment (and thus depth) at which the dura was punctured. Furthermore, the microdrive can be malfunctioning causing the electrodes not to lower, electrodes can bend, notebook keeping can be imperfect, the silence between cortical areas can be difficult to determine, the wrong electrode can be lowered etc. All these factors make it difficult to determine whether the electrode tip was located in the medial or in the lateral bank of the IPS, or in the anterior or posterior bank of the arcuate sulcus, or any other sulcus for that matter.

To improve electrode localization we combined high-resolution CT scanning with pre- and postoperative MRI imaging to localize individual electrode tips. We compared this method to the traditional method of notebook keeping, and verified our results by inducing metallic depositions using electrical stimulation at the end of the experiment.

## 4. Results

Using a multichannel electrode recording system requires a precise positioning of the recording system followed by an equally precise localization of the individual electrodes, especially when targeting multiple cortical areas.

### 4.1. Chamber visualization

The stereotactic coordinates of the chamber were calculated based on a preoperative MRI scan, in such a way that all cortical areas of interest could be accessed. The white outline in Fig. 1 mimics the outline of a 96-channel microelectrode recording system and is positioned in such a way that all parietal areas of interest (anterior intraparietal (AIP), lateral intraparietal (LIP), medial intraparietal (MIP) and posterior intraparietal area (PIP)) could be reached. The stereotactic coordinates of the center of the outline were determined and used for chamber implantation. After implantation of the chamber and before insertion of the microdrive, an MRI scan was obtained while a plug was inserted inside the chamber. Four custom-drilled holes inside this plug, filled with a contrast agent and thus visualized on MRI, allowed us to estimate the full extent of the microdrive. Fig. 2B (monkey S) shows the most anterior tube directed towards the anterior part of the intraparietal sulcus; the most posterior tube towards the posterior part of the intraparietal sulcus, and the most lateral tube towards the parietal convexity ventral to the IPS (note that the most medial tube was not visible). Thus, the microdrive with electrodes inserted inside the chamber can be targeted towards (almost) the entire intraparietal sulcus: from the anterior to the caudal IPS, including both the medial and the lateral bank. Similarly, the extent of a cylinder positioned over premotor/prefrontal cortex was visualized (Fig. 2C): monkey A had coverage from the central sulcus until the tip of the inferior part of the arcuate sulcus.

### 4.2. Electrode localization

Combining CT scans during the experiment with a preoperative MRI scan provides crucial information about the exact electrode location of multielectrode systems with individually moveable electrodes. A hybrid image (Fig. 3B) of the postoperative CT scan (Fig. 3A) and a

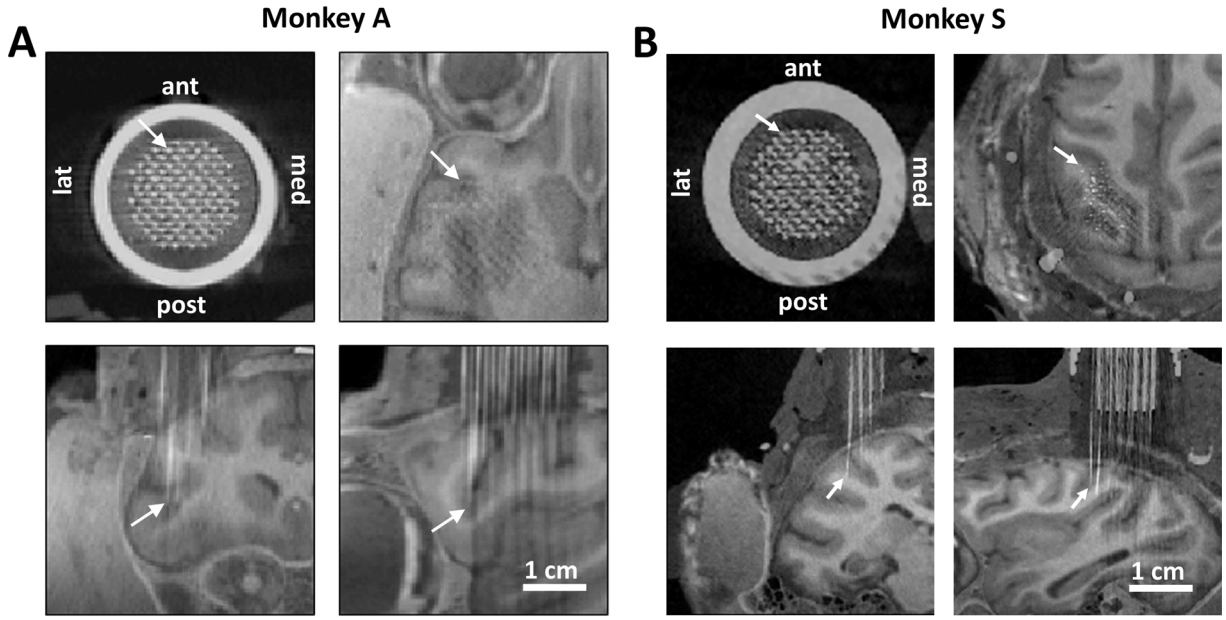


**Fig. 4.** Electrode localization examples for monkey A in frontal cortex (A) and monkey S in parietal cortex (B). The top left corner shows a top view of the microdrive with all 96 electrodes. The white arrow indicates one individual electrode, of which the tip is indicated with a white arrow in the CT/MRI fusion images (axial, coronal and sagittal).

preoperative MRI scan allows to identify individual electrodes and their exact position. The localization of an example premotor electrode is shown in Fig. 4 (monkey A). Individual electrodes can be identified on an axial CT slice (Fig. 4A, top left). The tip of the example electrodes (indicated with the white arrow) was, at the moment of the CT scan, located in the anterior part of the lower bank of the inferior ramus of the arcuate sulcus, corresponding to area 44 (Fig. 4A, top right & bottom). The same approach can be used for other cortical areas, such as parietal regions in Fig. 4B (monkey S): the arrow indicates the most lateral/anterior electrode, and the CT/MRI fusion image illustrates that this electrode has traversed the anterior lateral bank of the IPS (area AIP) and has reached white matter at the time of the CT scan. Note that the 96 individual channels can be linked to individual recording traces on the neural signal processor given that the electrode connection is identical on a daily base.

### 4.3. Cortex localization

Fig. 4 illustrates the importance of the current method for multi-electrode arrays targeting different cortical areas separated by a sulcus: both example electrodes (monkey S and monkey A) have travelled through cortex and sulcus to reach a second area, which response properties are typically very different from the first targeted area. Although the sulcus is usually defined by the lack neuronal activity, it can be difficult to determine the difference between cortex and sulcus (e.g. due to the presence of line noise). Our method can provide crucial additional information about this transition. Indeed, Fig. 5 shows the lab notes on the absence and presence of spiking activity over consecutive recording sessions (background activity, clear spiking activity or no clear activity (noise), example neuronal activity in the rightmost columns), relative to the electrode position at the moment of the CT scan. Our notes indicated four groups of recording sessions (Fig. 5: center): three individual sessions of spiking or background activity, followed by several sessions of silence; another period of background/spiking activity and a fourth period of silence. This corresponds with the electrode location as shown in our hybrid image (Fig. 5, left): medial bank of the IPS; sulcus; lateral bank; white matter. Fig. 5 thus illustrates that the information obtained from the hybrid image and the notes on spiking activity show a similar pattern, with the clear advantage of the visualization of the exact position (dorso-lateral and antero-posterior) of the electrode using our method.

### 4.4. Validation

Importantly, our method depends on a preoperative MRI scan, thus any changes in brain volume or structure during the experiment are unknown and cannot be incorporated in our method. To control for unexpected and unknown anatomical changes during the experiment, electrical stimulation was performed on a few selected electrodes at the end of one experiment before retracting the electrodes and removing the microdrive. This stimulation created metallic depositions, visible on MRI imaging (Fung et al., 1998) Fig. 6A shows the hybrid image of the final CT scan (in which the electrodes are at the same positions as where the lesions were made), and the white arrows indicate the selected electrodes. The post-experimental MRI images are shown in Fig. 6, with the white arrow indicating the metallic deposition made at the electrode tip. Although there seems to be a minimal deformation of the brain, Fig. 6 shows that the lesion was located close to the estimated location and thus validates our method as an important additional tool for electrode location.

## 5. Discussion

As spatially distributed patterns of synchronous activity play a fundamental role in cognitive neuroscience (Freeman and Skarda, 1985; Gray and Singer, 1989; Bressler, 1995; Gray and McCormick, 1996; Singer, 1999; Usrey and Reid, 1999; Azouz and Gray, 2000; Freeman, 2000; Maldonado et al., 2000; Varela et al., 2001; Buzsaki and Draguhn, 2004; Fries, 2005), the need to develop flexible multi-electrode recording systems is high. Large populations of neurons, distributed across widespread regions of the cortex, must rapidly and selectively cooperate in a flexible manner to enable a vast repertoire of possible functions (Mesulam, 1990; Bressler, 1995; Tononi and Edelman, 1998; Varela et al., 2001; Bressler and Menon, 2010).

Multielectrode recording devices with individually moveable electrodes can yield an exceptionally high number of unique recording sites in different cortical regions. For example, 100 electrodes in two cortical areas (2.5 mm thick) at both sides of a sulcus can yield 2000 unique

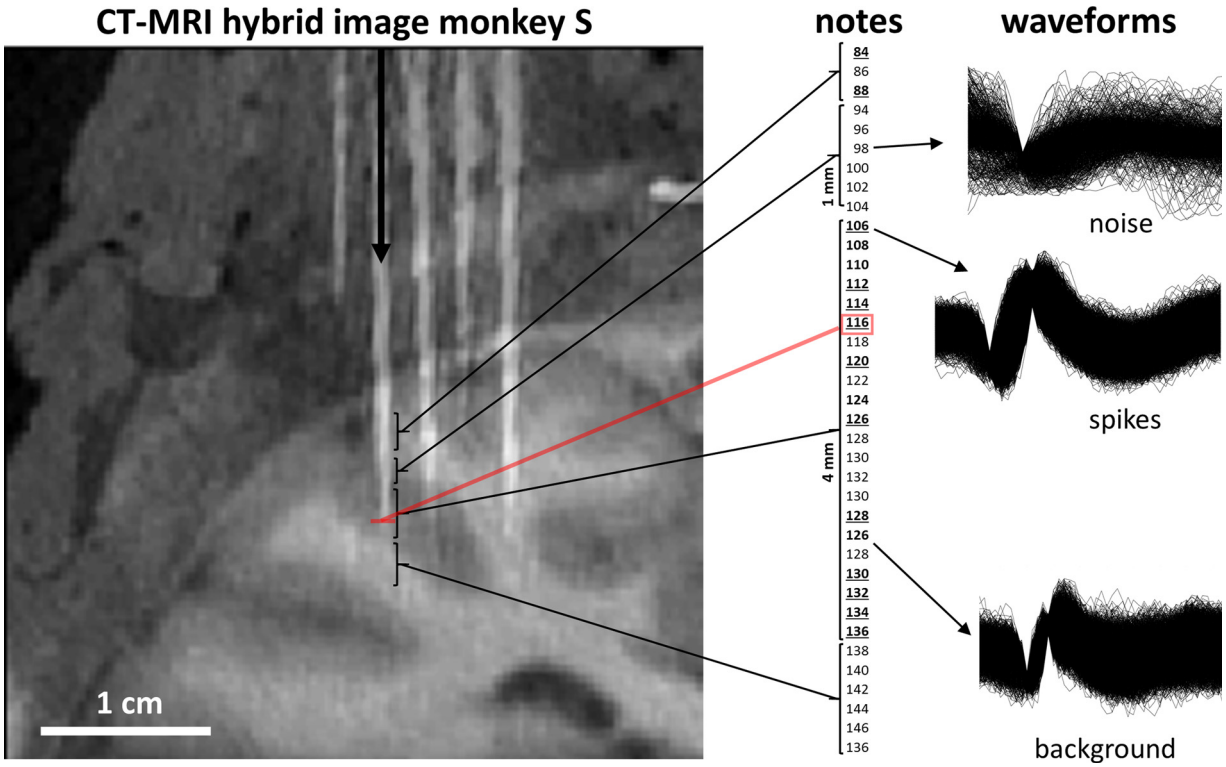


**Fig. 5.** Cortex localization: CT-MRI hybrid compared to notebook keeping. Left panel shows the CT/MRI hybrid image focused on the intraparietal sulcus. Black arrow indicates the electrode for which notes on the spiking activity are shown in the middle column. The red line indicates the electrode tip position, at which spiking activity was found (middle panel). Square brackets indicate, respectively, cortex, sulcus, cortex, white matter. The notes (middle column) refer to the electrode depth (number of turns: 8 turns = 1 mm) and type of recorded activity: bold + underline refers to spiking activity, bold refers to background activity, otherwise noise. Example waveforms of the three different patterns are shown on the right: noise, spikes, background activity.

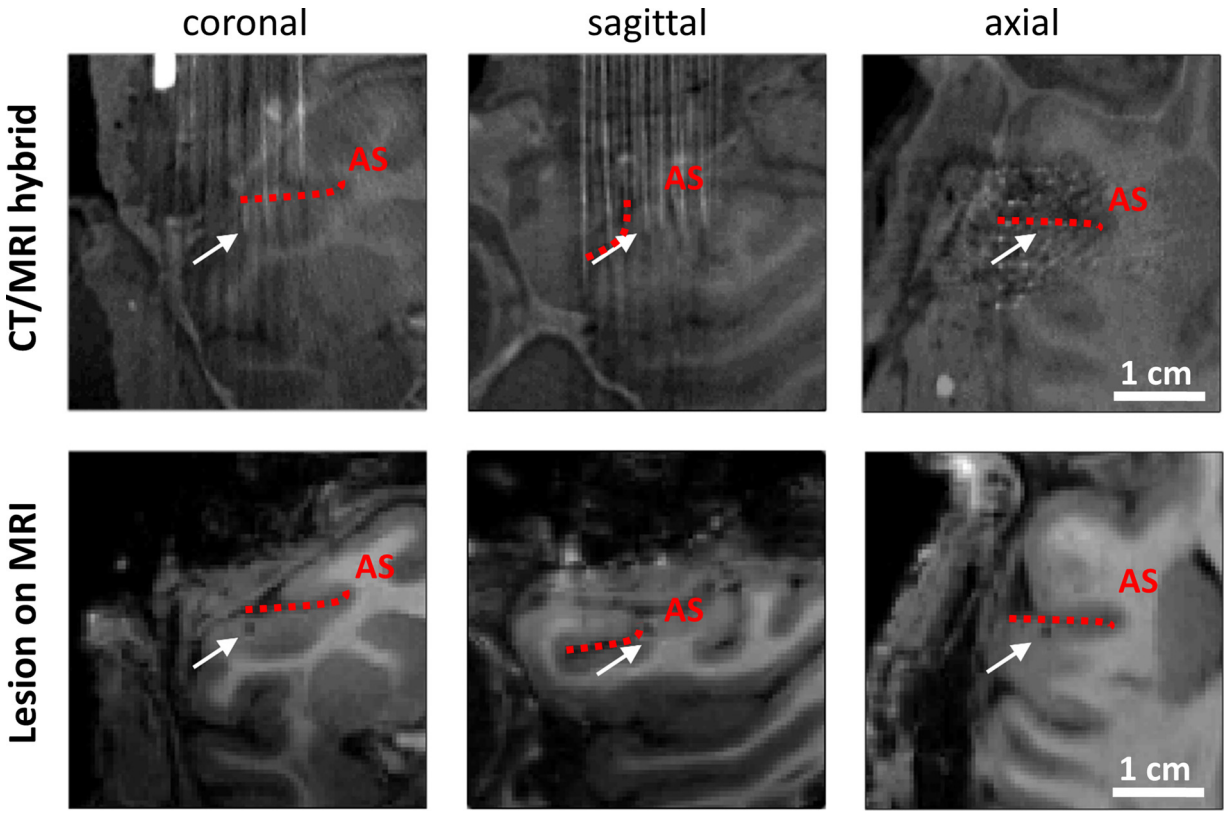


**Fig. 6.** Example of electrode metallic deposition after stimulation. The position of the electrode before lesioning is predicted on the CT/MRI hybrid images. After the lesion is performed, the microdrive was removed and an MRI scan was performed which shows the metallic deposition. The arcuate sulcus (AS) is depicted in red.

recording sites if we record every 250 micron across the cortical thickness. This is still an order of magnitude larger than other microelectrode arrays (Nordhausen et al., 1996; Maynard et al., 1999; Dickey et al., 2009) or recently developed laminar probes such as Neuropixel (Jun et al., 2017).

To record from multiple areas simultaneously, one does not only need a reliable recording system but also a reliable and validated method to estimate electrode tip locations. CT-MRI fusion is routinely used in neurosurgical applications, to localize electrodes (Darcey and Roberts, 2010; Lee et al., 2010; Geevarghese et al., 2016; Engelhardt et al., 2018), however to date, this technique has not been applied in animal studies with multi-electrodes microdrives. We have combined CT and MRI scanning for electrode localization and found a highly precise way of localizing electrodes and electrode tips of a multi-electrode system with individually moveable electrodes. We validated our technique by comparing with traditional localization methods based on notebook keeping, and by stimulation-induced metallic depositions at the electrode tips (which can be detected on a post-experimental MRI scan).

The steps described in this report are particularly relevant for the Gray Matter system, but can also be translated to other systems. The Gray Matter system requires the implantation of a cylinder, followed by a craniotomy and finally inserting the microdrive with electrodes a few days later. Our method consists of two steps: first, we use an anatomical T1 weighted structural image to estimate the outline of the microdrive (after chamber implantation but before microdrive insertion), followed by CT scans after microdrive insertion and electrode lowering. Obviously, these steps can be adjusted to fit the needs of individual research groups. Furthermore, research groups without the possibility of performing a CT scan but with access to an MRI scanner could visualize the extent of the chamber with more precision, i.e. instead of only four holes in the plug one could consider increasing the number of positions, matching the exact orientation of the electrodes, which can then be visualized using contrast agent in an MR scan. Although the methods presented here were only validated in rhesus macaques, a similar approach could be applied in rodents, as the resolution of our CT was adequate (0.6 mm) and MRI in rodents can be obtained at much higher field strengths (9 T or more), allowing the resolution of the MRI image to be in a similar range. Finally, a similar technique can be applied for other studies such as TMS-EcoG studies (Papazachariadis et al., 2014), where it is important to determine the position of the TMS-coil in reference to the EcoG-electrodes and the underlying cortical area(s). In the latter studies, coregistration of high-resolution CT (showing the EcoG electrodes) and MRI images will allow precise localization of the individual contact points.

Importantly, for our study we localized electrodes manually, i.e. we 'counted' the electrodes to localize the specific electrode we were interested in. This process could be simplified by the use of neuronavigation software and digitizing the electrodes. The latter will automatically segment the electrodes, allowing the user to simply select the electrode of interest. Although this process would be highly valuable for multielectrode recording systems with larger number of electrodes, specific software should be developed for this purpose.

While traditionally single electrode locations were visualized using histology at the end of the experiment (Yaxley et al., 1990; Vogels and Orban, 1994), nowadays the need for histology for electrode localization has tremendously decreased thanks to the availability of in vivo imaging with either CT or MRI (Popivanov et al., 2014; Premereur et al., 2015; Taubert et al., 2015). Due to their small diameter, single electrodes rarely leave visible tracks on MRI scans; therefore, electrophysiologists have sought a reliable method to mark the location of the recording positions. For histology, microlesions from electrical stimulation (Rolls et al., 1988; Colby et al., 1996) or inserting stainless steel wires (Vogels and Orban, 1994) have proven to be efficient; other research groups have injected nuclear yellow dye (Snyder et al., 1997) or horseradish peroxidase (Vogels and Orban, 1994). The most precise method to visualize the electrode location using MRI is to lower an electrode inside the brain towards the neuronal activations (Popivanov et al., 2014; Premereur et al., 2015; Taubert et al., 2015) or to create small metal depositions at the electrode tip (Fung et al., 1998). The latter technique is extremely useful for the post-hoc localization of the electrodes of a semi-chronic recording device.

We have used metal depositions to verify the CT/MRI mapping method by comparing the actual location of the electrode tip to the estimated one. Our results indicate that our method of combining CT scanning with a pre-operative MRI scan is reliable but obviously dependent on deformations of the brain occurring during the experiment (e.g. due to tissue growth between the dura and the plug). Manufacturers of chronic electrode recording systems, however, take great care of preventing such issues (Gray et al., 2007), and even if deformations have occurred, our method provides crucial information to reconstruct the electrode location at the end of the experiment. Indeed, the electrode endpoints (determined by metallic depositions) can be linked to the logged neural activity, and this can be extrapolated to neighboring electrodes.

Although the method presented here can be used to reliably estimate individual electrode localization throughout an experiment, additional tests may contribute to the localization of individual electrode tips. A combination of multiple metallic depositions (rather than five as in our study) on strategically chosen electrodes and electrode-depths, repeated CT-imaging throughout the experiment and histology at the end of the recordings will allow even better localization throughout and after the experiment.

## 6. Conclusions

In recent years, large semichronic multi-electrode recording systems with individually moveable electrodes for use in non-human primates have been developed. We present a method to precisely target brain areas using such recording systems and to localize the individual electrodes and electrode tips on each recording day. Our method uses a combination of preoperative MRI scanning and repeated CT scanning during the course of the experiment. Together with detailed notes about the neural activity on each recording day, we can reconstruct the electrode location throughout the entire experiment. The described technique allows for a precise anatomical identification of the recorded brain areas and thus to draw strong conclusions about the role of each targeted cortical area in the behavior under study.

## Declaration of Competing Interest

The authors declare no competing interests.

## Acknowledgments

We thank Stijn Verstraeten, Piet Kayenbergh, Gerrit Meulemans, Christophe Ulens and Inez Puttemans for technical assistance. We thank Astrid Hermans and Sara De Pril for administrative support.

This work was supported by Fonds Wetenschappelijk onderzoek (FWO) and Odysseus grant (KU Leuven). Tom Theys is supported by FWO (senior clinical researcher, FWO 1830717N).

## References

Azouz, R., Gray, C.M., 2000. Dynamic spike threshold reveals a mechanism for synaptic coincidence detection in cortical neurons in vivo. Proc. Natl. Acad. Sci. U.S.A. 97, 8110–8115.

Bastos, A.M., Loonis, R., Kornblith, S., Lundqvist, M., Miller, E.K., 2018. Laminar recordings in frontal cortex suggest distinct layers for maintenance and control of working memory. Proc. Natl. Acad. Sci. U.S.A. 115, 1117–1122.

Bressler, S.L., 1995. Large-scale cortical networks and cognition. Brain Res. Brain Res. Rev. 20, 288–304.

Bressler, S.L., Menon, V., 2010. Large-scale brain networks in cognition: emerging methods and principles. Trends Cogn. Sci. 14, 277–290.

Buschman, T.J., Miller, E.K., 2009. Serial, covert shifts of attention during visual search are reflected by the frontal eye fields and correlated with population oscillations. Neuron 63, 386–396.
Buzsaki, G., Draguhn, A., 2004. Neuronal oscillations in cortical networks. Science 304, 1926–1929.
Caprara, I., Premereur, E., Romero, M.C., Faria, P., Janssen, P., 2018. Shape responses in a macaque frontal area connected to posterior parietal cortex. NeuroImage 179, 298–312.
Colby, C.L., Duhamel, J.R., Goldberg, M.E., 1996. Visual, presaccadic, and cognitive activation of single neurons in monkey lateral intraparietal area. J. Neurophysiol. 76, 2841–2852.
Csicsvari, J., Henze, D.A., Jamieson, B., Harris, K.D., Sirota, A., Bartho, P., Wise, K.D., Buzsaki, G., 2003. Massively parallel recording of unit and local field potentials with silicon-based electrodes. J. Neurophysiol. 90, 1314–1323.
Darcey, T.M., Roberts, D.W., 2010. Technique for the localization of intracranially implanted electrodes. J. Neurosurg. 113, 1182–1185.
de Charms, R.C., Blake, D.T., Merzenich, M.M., 1999. A multielectrode implant device for the cerebral cortex. J. Neurosci. Methods 93, 27–35.
Dickey, A.S., Suminski, A., Amit, Y., Hatsopoulos, N.G., 2009. Single-unit stability using chronically implanted multielectrode arrays. J. Neurophysiol. 102, 1331–1339.
Donoghue, J.P., Sanes, J.N., Hatsopoulos, N.G., Gaal, G., 1998. Neural discharge and local field potential oscillations in primate motor cortex during voluntary movements. J. Neurophysiol. 79, 159–173.
Dotson, N.M., Goodell, B., Salazar, R.F., Hoffman, S.J., Gray, C.M., 2015. Methods, caveats and the future of large-scale microelectrode recordings in the non-human primate. Front. Syst. Neurosci. 9, 149.
Dotson, N.M., Hoffman, S.J., Goodell, B., Gray, C.M., 2017. A large-scale semi-chronic microdrive recording system for non-human Primates. Neuron 96, 769–782 e762.
Dykstra, A.R., Chan, A.M., Quinn, B.T., Zepeda, R., Keller, C.J., Cormier, J., Madsen, J.R., Eskandar, E.N., Cash, S.S., 2012. Individualized localization and cortical surface-based registration of intracranial electrodes. NeuroImage 59, 3563–3570.
Eliades, S.J., Wang, X., 2008. Chronic multi-electrode neural recording in free-roaming monkeys. J. Neurosci. Methods 172, 201–214.
Engelhardt, J., Guehl, D., Damon-Perriere, N., Branchard, O., Burbaud, P., Cuny, E., 2018. Localization of deep brain stimulation electrode by image registration is software dependent: a comparative study between four widely used software programs. Stereotact. Funct. Neurosurg. 96, 364–369.
Erickson, C.A., Desimone, R., 1999. Responses of macaque perirhinal neurons during and after visual stimulus association learning. J. Neurosci. 19, 10404–10416.
Feingold, J., Desrochers, T.M., Fujii, N., Harlan, R., Tierney, P.L., Shimazu, H., Amemori, K., Graybiel, A.M., 2012. A system for recording neural activity chronically and simultaneously from multiple cortical and subcortical regions in nonhuman primates. J. Neurophysiol. 107, 1979–1995.
Freeman, W.J., 2000. Mesoscopic neurodynamics: from neuron to brain. J. Physiol. Paris 94, 303–322.
Freeman, W.J., Skarda, C.A., 1985. Spatial EEG patterns, non-linear dynamics and perception: the neo-Sherringtonian view. Brain Res. 357, 147–175.
Fries, P., 2005. A mechanism for cognitive dynamics: neuronal communication through neuronal coherence. Trends Cogn. Sci. 9, 474–480.
Fries, P., Roelfsema, P.R., Engel, A.K., Konig, P., Singer, W., 1997. Synchronization of oscillatory responses in visual cortex correlates with perception in interocular rivalry. Proc. Natl. Acad. Sci. U.S.A. 94, 12699–12704.
Fujimoto, A., Okanishi, T., Kanai, S., Sato, K., Nishimura, M., Enoki, H., 2017. Real-time three-dimensional (3D) visualization of fusion image for accurate subdural electrodes placement of epilepsy surgery. J. Clin. Neurosci. 44, 330–334.
Fung, S.H., Burstein, D., Born, R.T., 1998. In vivo microelectrode track reconstruction using magnetic resonance imaging. J. Neurosci. Methods 80, 215–224.
Geevarghese, R., O'Gorman Tuura, R., Lumsden, D.E., Samuel, M., Ashkan, K., 2016. Registration accuracy of CT/MRI fusion for localisation of deep brain stimulation electrode position: an imaging study and systematic review. Stereotact. Funct. Neurosurg. 94, 159–163.
Gray, C.M., Goodell, B., Lear, A., 2007. Multichannel micromanipulator and chamber system for recording multineuronal activity in alert, non-human primates. J. Neurophysiol. 98, 527–536.
Gray, C.M., McCormick, D.A., 1996. Chattering cells: superficial pyramidal neurons contributing to the generation of synchronous oscillations in the visual cortex. Science 274, 109–113.
Gray, C.M., Singer, W., 1989. Stimulus-specific neuronal oscillations in orientation columns of cat visual cortex. Proc. Natl. Acad. Sci. U.S.A. 86, 1698–1702.
Gross, C.G., Rocha-Miranda, C.E., Bender, D.B., 1972. Visual properties of neurons in inferotemporal cortex of the Macaque. J. Neurophysiol. 35, 96–111.
Hinds, W.A., Misra, A., Sperling, M.R., Sharan, A., Tracy, J.I., Moxon, K.A., 2018. Enhanced co-registration methods to improve intracranial electrode contact localization. Neuroimage Clin. 20, 398–406.
Hoffman, K.L., McNaughton, B.L., 2002. Coordinated reactivation of distributed memory traces in primate neocortex. Science 297, 2070–2073.
Janssen, P., Vogels, R., Orban, G.A., 1999. Macaque inferior temporal neurons are selective for disparity-defined three-dimensional shapes. Proc. Natl. Acad. Sci. U.S.A. 96, 8217–8222.
Jun, J.J., Steinmetz, N.A., Siegle, J.H., Denman, D.J., Bauza, M., Barbarits, B., Lee, A.K., Anastassiou, C.A., Andrei, A., Aydin, C., Barbic, M., Blanche, T.J., Bonin, V., Couto, J., Dutta, B., Gratiy, S.L., Gutnisky, D.A., Hausser, M., Karsh, B., Ledochowitsch, P., Lopez, C.M., Mitelut, C., Musa, S., Okun, M., Pachitariu, M., Putzeys, J., Rich, P.D., Rossant, C., Sun, W.L., Svoboda, K., Carandini, M., Harris, K.D., Koch, C., O'Keefe, J., Harris, T.D., 2017. Fully integrated silicon probes for high-density recording of neural activity. Nature 551, 232–236.
Kaliukhovich, D.A., Vogels, R., 2012. Stimulus repetition affects both strength and synchrony of macaque inferior temporal cortical activity. J. Neurophysiol. 107, 3509–3527.
Kim, S., Normann, R.A., Harrison, R., Solzbacher, F., 2006. Preliminary study of the thermal impact of a microelectrode array implanted in the brain. Conference Proceedings : Annual International Conference of the IEEE Engineering in Medicine and Biology Society IEEE Engineering in Medicine and Biology Society Annual Conference 1. pp. 2986–2989.
Kipke, D.R., Vetter, R.J., Williams, J.C., Hetke, J.F., 2003. Silicon-substrate intracortical microelectrode arrays for long-term recording of neuronal spike activity in cerebral cortex. IEEE Trans. Neural Syst. Rehabil. Eng. 11, 151–155.
Kloosterman, F., Davidson, T.J., Gomperts, S.N., Layton, S.P., Hale, G., Nguyen, D.P., Wilson, M.A., 2009. Micro-drive array for chronic in vivo recording: drive fabrication. J. Vis. Exp.
Krupa, D.J., Wiest, M.C., Shuler, M.G., Laubach, M., Nicolelis, M.A., 2004. Layer-specific somatosensory cortical activation during active tactile discrimination. Science 304, 1989–1992.
Lawrence, B.M., Snyder, L.H., 2006. Comparison of effector-specific signals in frontal and parietal cortices. J. Neurophysiol. 96, 1393–1400.
Lee, J.Y., Kim, J.W., Lee, J.Y., Lim, Y.H., Kim, C., Kim, D.G., Jeon, B.S., Paek, S.H., 2010. Is MRI a reliable tool to locate the electrode after deep brain stimulation surgery? Comparison study of CT and MRI for the localization of electrodes after DBS. Acta Neurochir. 152, 2029–2036.
Maldonado, P.E., Friedman-Hill, S., Gray, C.M., 2000. Dynamics of striate cortical activity in the alert macaque: II. Fast time scale synchronization. Cereb. Cortex 10, 1117–1131.
Maynard, E.M., Hatsopoulos, N.G., Ojakangas, C.L., Acuna, B.D., Sanes, J.N., Normann, R.A., Donoghue, J.P., 1999. Neuronal interactions improve cortical population coding of movement direction. J. Neurosci. 19, 8083–8093.
Mendoza, G., Peyrache, A., Gamez, J., Prado, L., Buzsaki, G., Merchant, H., 2016. Recording extracellular neural activity in the behaving monkey using a semichronic and high-density electrode system. J. Neurophysiol. 116, 563–574.
Mesulam, M.M., 1990. Large-scale neurocognitive networks and distributed processing for attention, language, and memory. Ann. Neurol. 28, 597–613.
Murata, A., Gallese, V., Luppino, G., Kaseda, M., Sakata, H., 2000. Selectivity for the shape, size, and orientation of objects for grasping in neurons of monkey parietal area AIP. J. Neurophysiol. 83, 2580–2601.
Musallam, S., Bak, M.J., Troyk, P.R., Andersen, R.A., 2007. A floating metal microelectrode array for chronic implantation. J. Neurosci. Methods 160, 122–127.
Nelissen, K., Vanduffel, W., 2011. Grasping-related functional magnetic resonance imaging brain responses in the macaque monkey. J. Neurosci. 31, 8220–8229.
Nguyen, D.P., Layton, S.P., Hale, G., Gomperts, S.N., Davidson, T.J., Kloosterman, F., Wilson, M.A., 2009. Micro-drive array for chronic in vivo recording: tetrode assembly. J. Vis. Exp.
Nicolelis, M.A., Dimitrov, D., Carmena, J.M., Crist, R., Lehew, G., Kralik, J.D., Wise, S.P., 2003. Chronic, multisite, multielectrode recordings in macaque monkeys. Proc. Natl. Acad. Sci. U.S.A. 100, 11041–11046.
Nicolelis, M.A., Ghazanfar, A.A., Faggin, B.M., Votaw, S., Oliveira, L.M., 1997. Reconstructing the engram: simultaneous, multisite, many single neuron recordings. Neuron 18, 529–537.
Nordhausen, C.T., Maynard, E.M., Normann, R.A., 1996. Single unit recording capabilities of a 100 microelectrode array. Brain Res. 726, 129–140.
Papazachariadis, O., Dante, V., Verschure, P.F., Del Giudice, P., Ferraina, S., 2014. iTBS-induced LTP-like plasticity parallels oscillatory activity changes in the primary sensory and motor areas of macaque monkeys. PLoS One 9, e112504.
Poort, J., Self, M.W., van Vugt, B., Malkki, H., Roelfsema, P.R., 2016. Texture segregation causes early figure enhancement and later ground suppression in areas V1 and V4 of visual cortex. Cereb. Cortex 26, 3964–3976.
Popivanov, I.D., Jastorff, J., Vanduffel, W., Vogels, R., 2014. Heterogeneous single-unit selectivity in an fMRI-defined body-selective patch. J. Neurosci. 34, 95–111.
Premereur, E., Taubert, J., Janssen, P., Vogels, R., Vanduffel, W., 2016. Effective connectivity reveals largely independent parallel networks of face and body patches. Curr. Biol. 26, 3269–3279.
Premereur, E., Van Dromme, I.C., Romero, M.C., Vanduffel, W., Janssen, P., 2015. Effective connectivity of depth-structure-selective patches in the lateral bank of the macaque intraparietal sulcus. PLoS Biol. 13, e1002072.
Premereur, E., Vanduffel, W., Janssen, P., 2011. Functional heterogeneity of macaque lateral intraparietal neurons. J. Neurosci. 31, 12307–12317.
Premereur, E., Vanduffel, W., Janssen, P., 2012. Local field potential activity associated with temporal expectations in the macaque lateral intraparietal area. J. Cogn. Neurosci. 24, 1314–1330.
Roelfsema, P.R., Engel, A.K., Konig, P., Singer, W., 1997. Visuomotor integration is associated with zero time-lag synchronization among cortical areas. Nature 385, 157–161.
Rolls, E.T., Scott, T.R., Sienkiewicz, Z.J., Yaxley, S., 1988. The responsiveness of neurones in the frontal opercular gustatory cortex of the macaque monkey is independent of hunger. J. Physiol. 397, 1–12.
Romero, M.C., Pani, P., Janssen, P., 2014. Coding of shape features in the macaque anterior intraparietal area. J. Neurosci. 34, 4006–4021.
Rousche, P.J., Pellinen, D.S., Pivin Jr., D.P., Williams, J.C., Vetter, R.J., Kipke, D.R., 2001. Flexible polyimide-based intracortical electrode arrays with bioactive capability. IEEE Trans. Biomed. Eng. 48, 361–371.
Scherberger, H., Fineman, I., Musallam, S., Dubowitz, D.J., Bernheim, K.A., Pesaran, B., Corneil, B.D., Gilliken, B., Andersen, R.A., 2003. Magnetic resonance image-guided implantation of chronic recording electrodes in the macaque intraparietal sulcus. J. Neurosci. Methods 130, 1–8.

Schwarz, D.A., Lebedev, M.A., Hanson, T.L., Dimitrov, D.F., Lehew, G., Meloy, J., Rajangam, S., Subramanian, V., Ifft, P.J., Li, Z., Ramakrishnan, A., Tate, A., Zhuang, K.Z., Nicolelis, M.A., 2014. Chronic, wireless recordings of large-scale brain activity in freely moving rhesus monkeys. Nat. Methods 11, 670–676.

Singer, W., 1999. Neuronal synchrony: a versatile code for the definition of relations? Neuron 24 (49–65), 111–125.

Snyder, L.H., Batista, A.P., Andersen, R.A., 1997. Coding of intention in the posterior parietal cortex. Nature 386, 167–170.

Swadlow, H.A., Bereshpolova, Y., Bezdudnaya, T., Cano, M., Stoelzel, C.R., 2005. A multi-channel, implantable microdrive system for use with sharp, ultra-fine “Reitboeck” microelectrodes. J. Neurophysiol. 93, 2959–2965.

Takeda, M., Hirabayashi, T., Adachi, Y., Miyashita, Y., 2018. Dynamic laminar rerouting of inter-areal mnemonic signal by cognitive operations in primate temporal cortex. Nat. Commun. 9, 4629.

Taubert, J., Van Belle, G., Vanduffel, W., Rossion, B., Vogels, R., 2015. The effect of face inversion for neurons inside and outside fMRI-defined face-selective cortical regions. J. Neurophysiol. 113, 1644–1655.

Theys, T., Pani, P., van Loon, J., Goffin, J., Janssen, P., 2012. Selectivity for three-dimensional shape and grasping-related activity in the macaque ventral premotor cortex. J. Neurosci. 32, 12038–12050.

Theys, T., Pani, P., van Loon, J., Goffin, J., Janssen, P., 2013. Three-dimensional shape coding in grasping circuits: a comparison between the anterior intraparietal area and ventral premotor area F5a. J. Cogn. Neurosci. 25, 352–364.

Tononi, G., Edelman, G.M., 1998. Consciousness and complexity. Science 282, 1846–1851.

Tsao, D.Y., Freiwald, W.A., Tootell, R.B., Livingstone, M.S., 2006. A cortical region consisting entirely of face-selective cells. Science 311, 670–674.

Umilta, M.A., Brochier, T., Spinks, R.L., Lemon, R.N., 2007. Simultaneous recording of macaque premotor and primary motor cortex neuronal populations reveals different functional contributions to visuomotor grasp. J. Neurophysiol. 98, 488–501.

Usrey, W.M., Reid, R.C., 1999. Synchronous activity in the visual system. Annu. Rev. Physiol. 61, 435–456.

Varela, F., Lachaux, J.P., Rodriguez, E., Martinerie, J., 2001. The brainweb: phase synchronization and large-scale integration. Nat. Rev. Neurosci. 2, 229–239.

Venkatachalam, S., Fee, M.S., Kleinfeld, D., 1999. Ultra-miniature headstage with 6-channel drive and vacuum-assisted micro-wire implantation for chronic recording from the neocortex. J. Neurosci. Methods 90, 37–46.

Verhoef, B.E., Vogels, R., Janssen, P., 2011. Synchronization between the end stages of the dorsal and the ventral visual stream. J. Neurophysiol. 105, 2030–2042.

Vogels, R., Orban, G.A., 1994. Activity of inferior temporal neurons during orientation discrimination with successively presented gratings. J. Neurophysiol. 71, 1428–1451.

Wilson, M.A., McNaughton, B.L., 1993. Dynamics of the hippocampal ensemble code for space. Science 261, 1055–1058.

Yaxley, S., Rolls, E.T., Sienkiewicz, Z.J., 1990. Gustatory responses of single neurons in the insula of the macaque monkey. J. Neurophysiol. 63, 689–700.